Tellus (1996), 48A, 179–192
Printed in Belgium – all rights reserved

TELLUS
ISSN 0280–6495

Tracer budgets in the warm water sphere

By JAMES C. MCWILLIAMS, GOKHAN DANABASOGLU and PETER R. GENT*,
National Center for Atmospheric Research, PO Box 3000, Boulder, Colorado 80307, USA

(Manuscript received 26 January 1995; in final form 14 June 1995)

ABSTRACT

In global equilibrium numerical solutions for the oceanic general circulation, we examine the time-mean budgets for the tracers potential temperature and salinity integrated over volumes bounded by interior surfaces of constant tracer values and lying within the warm water sphere. In this domain, the budgets have surface fluxes primarily of one sign that must be balanced by mesoscale and microscale fluxes through its lower boundary, because advection makes a zero integral contribution. The mesoscale fluxes are represented by the isopycnally oriented, quasi-adiabatic parameterization of Gent and McWilliams and contribute little to the integral budgets where isopycnals are nearly tangent to the volume boundary. The microscale fluxes occur with a small vertical diffusivity ($\kappa_v = O(10^{-5})\,m^2\,s^{-1}$) in the predominantly stably stratified warm water sphere, yet they are shown to be sufficient to provide the primary balance against surface forcing in all ocean basins and over a wide range of tracer values. This is especially true for potential temperature because of the close alignment of isotherms and isopycnals. For salinity, however, the mesoscale isopycnal diffusion also contributes significantly to the budget. The budgets are dominated by the surface and interior fluxes from the time-mean circulation, although there are also modest contributions from the rectification of the seasonal cycle. These results are in contrast to previous analyses that concluded that much larger vertical diffusivities are required for budget balance. We do not attempt to fully resolve the relatively smaller role of vertical diffusion in other budget volumes outside the warm water sphere.

1. Introduction

There is a particular class of time-averaged, volume-integrated budgets for tracers in the global ocean circulation that poses a sharp conundrum with respect to diapycnal fluxes (i.e., across density surfaces). Although we focus here on the tracers potential temperature and salinity, a similar conundrum applies to any other tracer that has a strong meridional contrast in its surface flux. This budget class occurs in the tropics and subtropics for volumes bounded by the ocean surface, possibly the solid-earth boundary, and a surface of constant tracer value that outcrops at middle latitudes. (Such a surface is well defined in a coarse-grain sense, even if not microscopically.) The tracer forcing at the upper surface is predominantly of one sign if the outcropping boundary does not extend too far poleward, e.g., net heating for temperature and net evaporation for freshwater. So there is a tendency for net accumulation that must on average be balanced by a flux across the lower boundary. There can be no net advective transport across such a surface because of mass conservation. Furthermore, if the iso-tracer surface is also nearly an isopycnal (or neutral) surface, then mesoscale transport processes will be inefficient at providing the necessary tracer flux because they are nearly parallel to isopycnals. Thus, diapycnal transport due to sub-mesoscale motions provides the most likely means of balancing the net surface input for this volume. In addition, this volume is persistently stably stratified due to the net surface heating,

* Corresponding author.

and it contains relatively little and quite shallow convection (compared to more polar regions), which precludes any significant budget contribution from this efficient transport process. The relevant diapycnal diffusivities are those for stably stratified, interior regions. These have been estimated from local measurements of microstructure variance and purposeful tracer releases (Gregg, 1987; Ledwell et al., 1993; Ledwell and Watson, 1994; Toole et al., 1994) to be smaller than many analysts believe is consistent with balancing this class of tracer budgets (e.g., Walin, 1982; Li et al., 1984; Hogg, 1987; Olbers and Wenzel, 1989; de Szoeke, 1995). An exception is the tropical Pacific heat budget analysis of Niiler and Stevenson (1982), where consistency with microstructure measurements was found. Some have suggested that there must be an unmeasured, and possibly as yet unidentified, process with larger diapycnal diffusivities of global consequence e.g., mixing near lateral boundaries (Armi, 1978; Garrett, 1991), which may be at least locally significant for iso-tracer volumes contained within deep basins (Hogg et al., 1982). As a caution against such inferences, though, Davis (1994) points out that the sampling uncertainties in these empirical budget analyses are quite large.

The conundrum, therefore, is how to reconcile the apparent contradiction that arises from the conspiracy of circumstances described above. The geographical location of these volumes is within the warm water sphere, or Warmwassersphäre as defined by Wüst (1949). We will designate this class of budgets by this name because we suspect that he and his colleagues (Defant and Dietrich, in particular) had some appreciation of this conundrum. At the largest extent of the warm water sphere as he defined it, out to the 10°C potential temperature surface, the conundrum is less acute for the following reasons: (a) the surface forcing is not as strongly of one sign, thus less heat needs to be transported across the interior boundary; (b) isothermal surfaces are less coincident with isopycnal ones, thus permitting larger mesoscale fluxes across the interior boundary; and (c) the interior boundary is more frequently penetrated by convection with large diapycnal diffusivities, thus relieving the onus on stable-layer vertical fluxes. These ameliorating effects on the budget conundrum increase as the outcropping boundary extends farther poleward. Furthermore, fluxes in the bottom boundary layer may also play a significant role in budgets for even colder or fresher tracer volumes that have large lines of intersection with the bottom (see above).

We assess this conundrum by analyzing global equilibrium model solutions with a parameterization of mesoscale tracer transport that contributes nothing to diapycnal fluxes in a warm water sphere budget (Gent and McWilliams, 1990; Gent et al., 1995); the other parameterizations are conventional ones for horizontal and vertical momentum diffusion and vertical tracer diffusion. One particular solution, with mean seasonal-cycle forcing, has been shown to have fairly realistic tracer distributions and time- and zonal-mean meridional and surface tracer fluxes (Danabasoglu et al., 1994; Danabasoglu and McWilliams, 1995). Its diapycnal tracer diffusivity, κ_v, is $5 \times 10^{-5}\ m^2\ s^{-1}$ everywhere except in convective regions where it is much larger. This is smaller than typical values inferred from empirical tracer budgets, and it is also on the small end of the range previously used in oceanic general circulation models. Nevertheless, it is more than a factor of two larger than the estimates from tracer-release experiments (Ledwell et al., 1993; Ledwell and Watson, 1994). We have used this larger-than-observed value so that the implicit diffusion due to numerical truncation error is small compared to the explicit, physical diffusion (Yin and Fung, 1991), given our relatively sparse vertical grid with only 20 levels. Here we augment this with two more solutions. The first has steady forcing, because we will see that the essential character of the mean tracer budget balance is preserved with this simplification. The second has both steady forcing and a closer-to-observed $\kappa_v = 2.5 \times 10^{-5}\ m^2\ s^{-1}$ with a corresponding increase in resolution to 40 vertical levels. If, instead, one were to examine warm water sphere tracer budgets in model solutions with the conventional, but physically implausible, mesoscale parameterization of horizontal tracer diffusion, then this would provide a substantial diapycnal flux mechanism that would relieve the uniqueness of the role of κ_v in balancing surface fluxes, and thus largely obviate the conundrum.

The contents of the paper are the following: the mathematical formulation of the tracer budgets (Section 2), the model solutions (Section 3), the budget analyses (Section 4), and a discussion of the results (Section 5).

2. Formulation of the tracer budgets

Consider a model whose tracer equations have the form

$$\tau_t + \nabla \cdot (\boldsymbol{u}\tau) = \mathscr{M}[\tau] + (\kappa_v \tau_z)_z, \tag{1}$$

for τ a generic tracer and $\boldsymbol{u}$ the three-dimensional velocity vector. The spatial coordinates are (x, y, z), time is t, and subscripts denote partial derivatives. We will consider only $\tau = \theta$ (potential temperature) and S (salinity) here. The final term in (1) is vertical diffusion, which is nearly equivalent to diapycnal diffusion where the isopycnal surfaces have small slope relative to level surfaces; the diffusivity values are different in stably and unstably stratified regions, as described above. The operator $\mathscr{M}$ represents transport by unresolved mesoscale eddy motions. Its form was proposed by Gent and McWilliams (1990) and recast by Gent et al. (1995) to be

$$\mathscr{M}[\tau] = -\nabla \cdot (\boldsymbol{u}^*\tau) + \mathscr{R}[\kappa_i, \tau], \tag{2}$$

where $\boldsymbol{u}^*$ is the non-divergent eddy-induced transport velocity,

$$\boldsymbol{u}^* = ((\kappa_i \rho_x/\rho_z)_z, (\kappa_i \rho_y/\rho_z)_z, -(\kappa_i \rho_x/\rho_z)_x - (\kappa_i \rho_y/\rho_z)_y). \tag{3}$$

The effect on τ can equivalently be interpreted as either diffusion of isopycnal layer thickness or the eddy-induced transport associated with the inhomogeneous, anti-symmetric component of a diffusion tensor. Here ρ is the potential density with a local reference pressure, and $\mathscr{R} \equiv \nabla \cdot \boldsymbol{R}$ represents diffusion of τ along isopycnals with coefficient κ_i (e.g., Redi, 1982; Gent and McWilliams, 1990). In the solutions here we make the simple choice of uniform $\kappa_i = 10^3\ \mathrm{m^2\,s^{-1}}$, which is roughly consistent with observations of float dispersion (McWilliams et al., 1983; Böning, 1988). The boundary conditions on (1)–(3) are a surface flux at $z = 0$,

$$\kappa_v \tau_z = Q^\tau, \tag{4}$$

where Q^τ is the flux of τ into the ocean, and zero-flux conditions for mass and tracers for all other transport processes at all solid-earth boundaries.

Now consider a warm water sphere tracer budget, schematically indicated in Fig. 1. It is

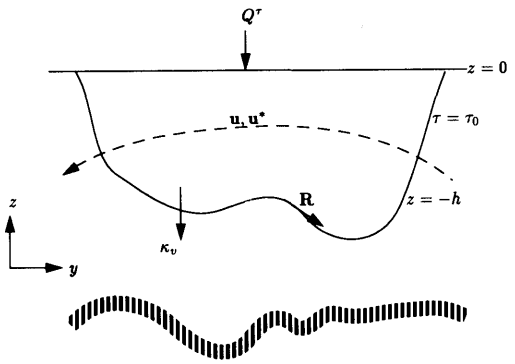

Fig. 1. Schematic of contributions to a tracer budget in the warm water sphere.

derived by integrating (1) over a volume $\mathscr{V}$ bounded by $\delta\mathscr{V}$ consisting of $z = 0$, $z = -h(x, y, t)$ at which $\tau(x, y, t) = \tau_0$, and any solid-earth surface at which $\tau > \tau_0$. If we consider a steady solution with steady surface fluxes, then the tendency term vanishes. By Gauss' integral theorem,

$$\int_{\mathscr{V}} \nabla \cdot (\boldsymbol{U}\tau)\, \mathrm{d}V = \int_{\delta\mathscr{V}} \tau \boldsymbol{U} \cdot \hat{\boldsymbol{n}}\, \mathrm{d}A$$

$$= \int_{\tau = \tau_0} \tau \boldsymbol{U} \cdot \hat{\boldsymbol{n}}\, \mathrm{d}A$$

$$= \tau_0 \int_{\tau = \tau_0} \boldsymbol{U} \cdot \hat{\boldsymbol{n}}\, \mathrm{d}A = 0,$$

where $\boldsymbol{U}$ is either velocity vector in (1)–(3) and $\hat{\boldsymbol{n}}$ is a unit outward normal vector on $\delta\mathscr{V}$. The second line follows because $\boldsymbol{U} \cdot \hat{\boldsymbol{n}} = 0$ at $z = 0$ and all solid-earth boundaries. The final result is a consequence of non-divergence of $\boldsymbol{U}$ and thus integral mass conservation across any closed material surface. Therefore, the integrated advections also vanish. Note that this result does not depend on the mutual orientation of the velocity vectors and the iso-tracer surface, and in general we do not expect alignment between them. However, under the circumstances of nearly steady solutions, near alignment of isopycnal and iso-tracer surfaces, and small vertical diffusion in the interior, then (1)–(2) imply that $\boldsymbol{u} + \boldsymbol{u}^*$ is nearly tangential to the iso-tracer surface.

The resulting budget is

$$0 = \int_{\mathscr{V}} (\kappa_v \tau_z)_z\, \mathrm{d}V + \int_{\mathscr{V}} \mathscr{R}[\kappa_i, \tau]\, \mathrm{d}V,$$

or

$$0 = \int_{z=0} Q^{\tau}\, \mathrm{d}A - \int_{\tau=\tau_0} \kappa_v \tau_z\, \mathrm{d}A + \int_{\tau=\tau_0} \boldsymbol{R}\cdot\hat{\boldsymbol{n}}\, \mathrm{d}A, \tag{5}$$

where $\boldsymbol{R}\cdot\hat{\boldsymbol{n}}$ is zero at the surface. (5) shows that the surface forcing is balanced by the vertical and isopycnal diffusive fluxes through the lower boundary in the interior. Finally, insofar as the $\tau=\tau_0$ surface nearly coincides with an isopycnal surface, as tends to be particularly true for θ in the warm water sphere, then $\boldsymbol{R}\cdot\hat{\boldsymbol{n}}\approx 0$, which implies a balance in (5) primarily between surface forcing and vertical flux at the lower boundary.

We can generalize the budgets to transient solutions with transient surface fluxes. Again consider an integral of the instantaneous tracer equation (1) over an instantaneous volume $\mathscr{V}$ enclosed by $z=0$, $\tau=\tau_0$, and any solid-earth boundary at which $\tau>\tau_0$. For the same reasons as above, advection can contribute nothing to this budget and isopycnal diffusion will contribute little when isopycnal and iso-tracer surfaces are nearly coincident. The additional contribution is a tracer storage tendency term, $\int_{\mathscr{V}} \tau_t\, \mathrm{d}V$, that enters on the left-hand side of (5). If we now take a time average of the transient budget equation, then for each of the four contributing terms there is the possibility of "rectification" of budget fluctuations, RE. This we define as the difference between the time-averaged budget terms and these terms calculated with the time-averaged variables and the time-averaged location of the τ_0 surface. For example, for the vertical flux at the bottom boundary, we may write

$$\mathrm{RE} \equiv \overline{\int_{\tau=\tau_0} \kappa_v \tau_z\, \mathrm{d}A} - \int_{\bar{\tau}=\tau_0} \kappa_v \bar{\tau}_z\, \mathrm{d}A. \tag{6}$$

RE arises from correlation between fluctuations in the location of the budget integration volume and the integrand. Analogous relations to (6) exist for the other budget terms, and only for the storage tendency term is there no contribution from the mean component, because $\bar{\tau}_t = 0$.

One might alternatively consider a tracer budget volume bounded by an isopycnal rather than iso-tracer surface. The contribution from $\mathscr{R}$ would be zero, but the advection contributions would be nonzero in the heat and freshwater budgets. If the equation of state had a linear relation between potential density and θ and S, then potential density (or buoyancy) would also be a tracer in this context, and the buoyancy budget would have zero contributions from both advection and isopycnal diffusion. However, with the more general equation of state of sea water, additional transport processes can contribute (e.g., cabbeling) and no simplification comparable to (5) would apply. Also, there are ambiguities associated with the definition of a global, neutrally buoyant, potential density surface (McDougall, 1987). For all these reasons, we focus on iso-tracer surfaces to more cleanly confront the budget conundrum. In practice, though, an isothermal surface is not very different from an isopycnal one in the warm water sphere.

In the model discretization, the tracer budget integrands are evaluated at the tracer grid points. For each grid point a volumetric weight is defined as the fraction of the cell within the iso-tracer volume, using linear interpolation between tracer grid-point values to determine the volume boundary. A discrete volume integral is the sum of grid-point integrand times the volumetric weight times the cell volume.

3. Solutions

We will analyze 3 solutions, each of which has been integrated for $O(10^4)$ years to reach equilibrium. The first of these has been analyzed extensively in other papers, where it is designated either ISO (Danabasoglu et al., 1994) or I1 (Danabasoglu and McWilliams, 1995). Its computational grid spacing is 4° in longitude and 3° in latitude, and it has 20 levels in the vertical with grid spacing monotonically increasing from 50 m near the upper surface to about 450 m near the bottom. Its forcing fields are the seasonal cycles of wind stress from the ECMWF (1993) climatology and of buoyancy fluxes resulting from restoring at the surface to observed θ and S (Levitus, 1982). Here we will refer to it as case V5′, indicating its κ_v value of $5\times10^{-5}\ \mathrm{m^2\,s^{-1}}$ and its time-dependent forcing. A companion solution, case $\overline{\mathrm{V5}}$, is posed

identically to V5′ except that the forcing fields are held steady at their annual mean values. Finally, we also have computed case $\overline{V2.5}$, with steady forcing fields, $\kappa_v = 2.5 \times 10^{-5}\ m^2\ s^{-1}$, and twice as many vertical grid levels distributed by halving each of the V5 grid cells.

In equilibrium, the solution V5′ is periodic and both $\overline{V5}$ and $\overline{V2.5}$ are steady. This makes the time-mean budget analysis considerably simpler for the latter two solutions, and, as we will show, it has essentially the same character in all three solutions. Differences in the time-mean fields of solutions V5′ and $\overline{V5}$ are relatively small, especially in the warm water sphere away from the regions of deep convection, but there is a modest sensitivity to the different value of κ_v in $\overline{V2.5}$, as expected from the idealized-geometry solutions of Bryan (1987). In this section we make a brief comparison among the solutions $\overline{V5}$ and $\overline{V2.5}$ explicitly, and the solution V5′, whose analogous plots can be found in Danabasoglu and McWilliams (1995).

The vertically integrated (barotropic), horizontal transport streamfunction is quite similar in all cases, and especially so in the Northern Hemisphere and the tropics. In the Southern Hemisphere both the midlatitude gyres and the Antarctic Circumpolar Current (ACC) are somewhat weaker in $\overline{V2.5}$. The volume transport through Drake Passage is 128, 133, and 112 Sv (i.e., $10^6\ m^3\ s^{-1}$) in cases V5′, $\overline{V5}$, and $\overline{V2.5}$, respectively.

Fig. 2 shows the zonal mean potential temperature for cases $\overline{V5}$ and $\overline{V2.5}$. The solution from case V5′ is very similar to Fig. 2a. The main thermocline in the upper kilometer is somewhat sharper in $\overline{V2.5}$ than in $\overline{V5}$, as is expected because of the smaller vertical diffusivity. This shows that some degree of compensation occurs to maintain the diapycnal flux when κ_v is reduced. The sharper main thermocline in $\overline{V2.5}$ is in better agreement with the Levitus (1982) data than are cases V5′ and $\overline{V5}$, although all these solutions are substantial improvements over analogous solutions with horizontal tracer diffusion (Danabasoglu et al., 1994; Danabasoglu and McWilliams, 1995). The better agreement in θ in $\overline{V2.5}$ extends all the way to the surface. Given the surface boundary condition of restoration to the Levitus data, this means that the surface heat fluxes in $\overline{V2.5}$ are smaller than in $\overline{V5}$. As a consequence, less heat has to be transported poleward in $\overline{V2.5}$ than in $\overline{V5}$. This is

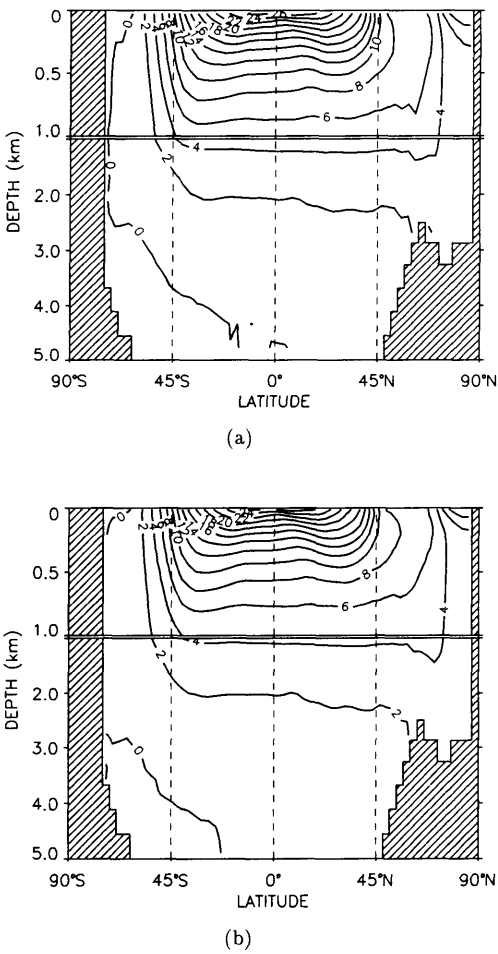

Fig. 2. Zonal – mean potential temperature distribution for the steady solutions with (a) $\kappa_v = 5 \times 10^{-5}\ m^2\ s^{-1}$ ($\overline{V5}$) and (b) $2.5 \times 10^{-5}\ m^2\ s^{-1}$ ($\overline{V2.5}$).

illustrated in Fig. 3a, which shows the northward heat transport for the three cases. The transport extrema in $\overline{V2.5}$ are about 80% of those in V5′. The small difference between V5′ and $\overline{V5}$ in the Northern Hemisphere is due to modest changes in the North Atlantic deep convection pattern in the seasonally varying and steady forcing cases. The surface freshwater fluxes are also somewhat smaller in $\overline{V2.5}$, so that less poleward transport of freshwater is required in this case (Fig. 3b). The reduced poleward tracer transports in $\overline{V2.5}$ are associated with a weaker mean meridional overturning circulation. The zonally integrated merid-

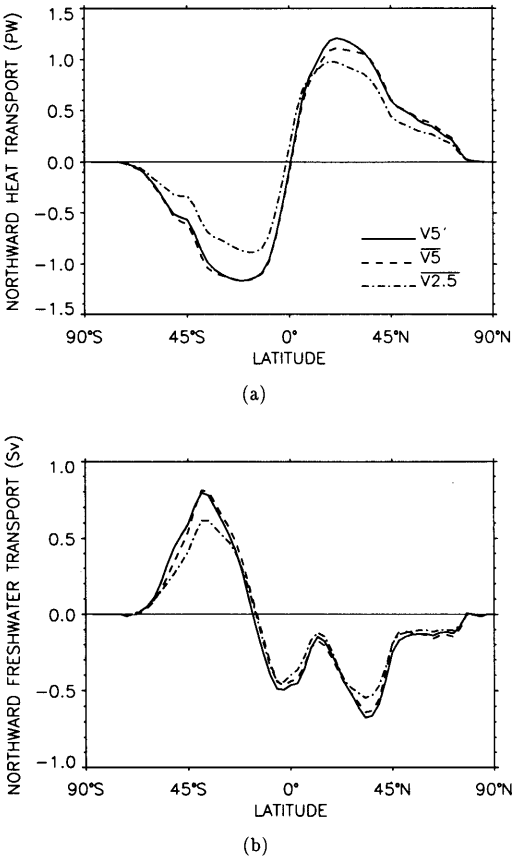

Fig. 3. Northward (a) heat and (b) freshwater transports for all three solutions.

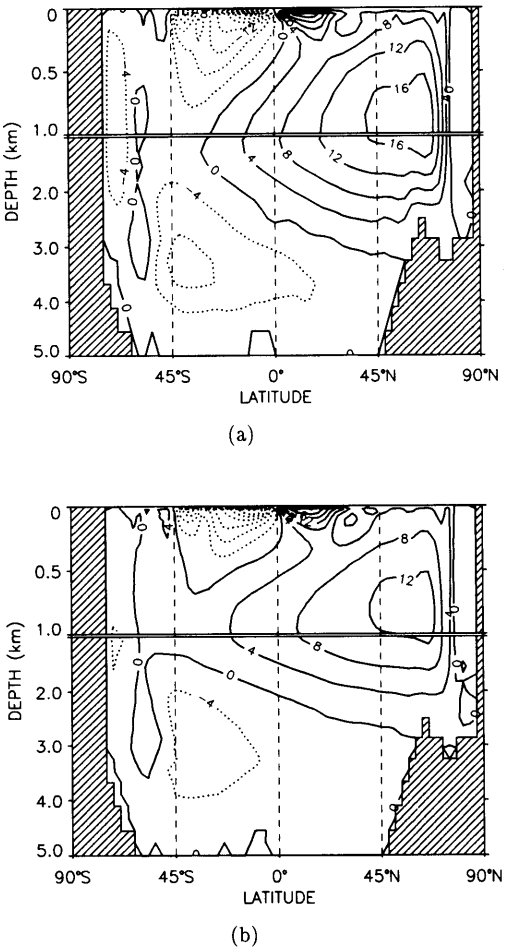

Fig. 4. Zonal – mean effective transport streamfunction for the steady solutions (a) $\overline{V5}$ and (b) $\overline{V2.5}$.

ional overturning streamfunctions, calculated from the effective transport velocity $\boldsymbol{u}+\boldsymbol{u}^*$ are shown in Fig. 4 for $\overline{V5}$ and $\overline{V2.5}$. The $\overline{V5}$ streamfunction is very similar to that for V5′.

The sharper main thermocline, reduced surface fluxes with consequent weaker poleward transport, and meridional overturning circulation in $\overline{V2.5}$ are consistent with the results of Bryan (1987). These effects are mainly a consequence of the artificial tracer surface boundary conditions, viz., restoration to observations, whereby the fluxes are determined by the discrepancy between computed and observed surface tracer values. Nevertheless, this type of boundary condition is the one most frequently used in global oceanic simulations, for lack as yet of a more reliable alternative. We could no doubt diminish the flux differences between $\overline{V5}$ and $\overline{V2.5}$ by decreasing the restoring time constant in the latter, but our purpose here is only to expose the sensitivity to κ_v, and not to engage in a tuning exercise to find the most realistic simulations for each κ_v.

Yin and Fung (1991) give the formula for the erroneous numerical diffusion κ_n due to vertical advection on a non-uniform grid with the discrete advection operator used in the model. We have evaluated κ_n for the solutions within the warm water sphere budget volumes analyzed below. (κ_n is larger in deep convection regions, but there the physical diffusivity is very much larger, so the error is not significant.) For cases $\overline{V5}$ and $\overline{V2.5}$,

respectively, the pointwise maximum κ_n values are about 7 and 2×10^{-5} m^2 s^{-1} (depending weakly on which budget volume) and the rms values are about ten times smaller, compared to the explicit κ_v values of 5 and 2.5×10^{-5} m^2 s^{-1}. Thus, we judge our resolution to be adequately accurate almost everywhere, but clearly any pursuit of solutions with smaller κ_v requires finer vertical grids.

Convection does not occur within any of the tracer volumes analyzed below for the solutions with steady forcing ($\overline{V5}$ and $\overline{V2.5}$). Even though there are some interior locations with negative surface buoyancy forcing, the uppermost grid volume is deep enough (50 m) and the other transport processes effective enough that the solution remains at least marginally stable. For V5′ there is some convection forced by the seasonal cycle, and its transport effects are included in the vertical diffusion budget term; however, convection so rarely penetrates these iso-tracer surfaces that its budget contribution is not significant compared to diffusion in stably stratified fluid.

4. Budgets

We first consider the heat budgets within volumes bounded by isotherms with $\theta_0 \geqslant 19$°C, where the surface heat flux is primarily of one sign, in order to focus on the conundrum stated in Section 1; budgets for lower θ_0 values are discussed below. (See Speer and Tziperman (1992, Fig. 1) for analogous estimates of the net buoyancy forcing as a function of density surface in the Atlantic.) The heat budgets for solution $\overline{V5}$ are shown in Fig. 5, separately for the Atlantic and

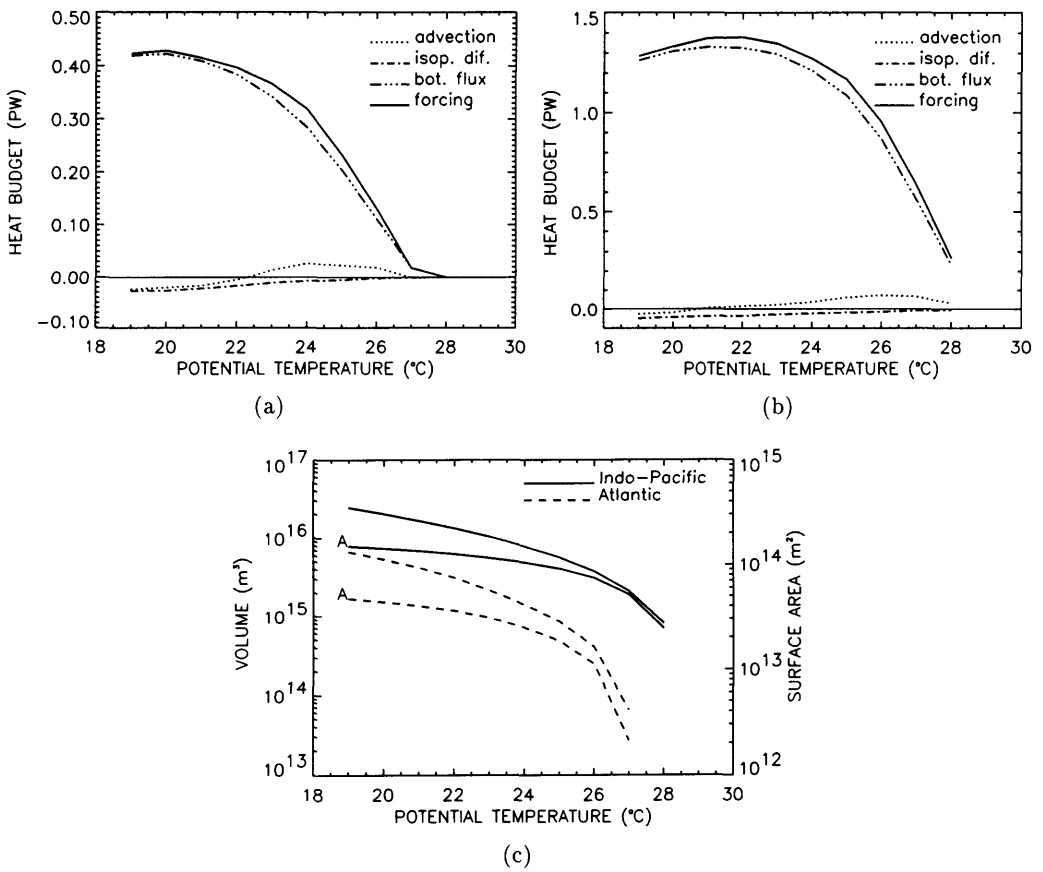

Fig. 5. Heat budget as a function of θ_0 in (a) Atlantic and (b) Indo – Pacific basins for the solution $\overline{V5}$. Also shown are (c) the surface area (lines connected to A) and volume contained within the bounding θ_0 surface.

Indo-Pacific basins. Because of the Indonesian passage, the Indian and Pacific budget volumes are not separate until $\theta_0 \geq 29°C$, where they become very small. For all θ_0, the balance is primarily between upper surface heating and lower boundary vertical heat flux, with only a small ($<10\%$) contribution from isopycnal diffusion (see eq. (5)), because of the near-alignment of isopycnal and isothermal surfaces in the warm water sphere. Also plotted is the total heat advection by the effective transport velocity, $\boldsymbol{u}+\boldsymbol{u}^*$, which theoretically should be zero and thus is an indication of the spatial discretization error in this budget calculation. It is small enough to permit the preceding conclusion, but large enough to make doubtful the quantitative estimate of $\boldsymbol{R}$. The variation of the budget volume with θ_0 is shown in Fig. 5c.

For the $\theta_0 = 20°C$ budget, the depth of the bounding surface (h; Fig. 6a) shows that this volume spans the tropics and sub-tropics in all oceans. The associated Q^θ (Fig. 6b) shows widespread tropical heating, weak fluxes throughout most of the subtropics, and strong cooling near the Gulf Stream, Kuroshio, and Agulhas currents. The vertical diffusion across the lower boundary is proportional to θ_z; its horizontal pattern (Fig. 6c) is highly inhomogeneous, which indicates why it may be difficult to accurately estimate heat budgets observationally. The largest θ_z values (up to $0.14°C\ m^{-1}$) occur in the eastern tropical oceans and along the subtropical western boundaries. The Indonesian throughflow contributes about 0.15 PW of heat transfer from the Pacific to the Indian basin within the $\theta_0 = 20°C$ volume. This is about as large as the surface heating in the

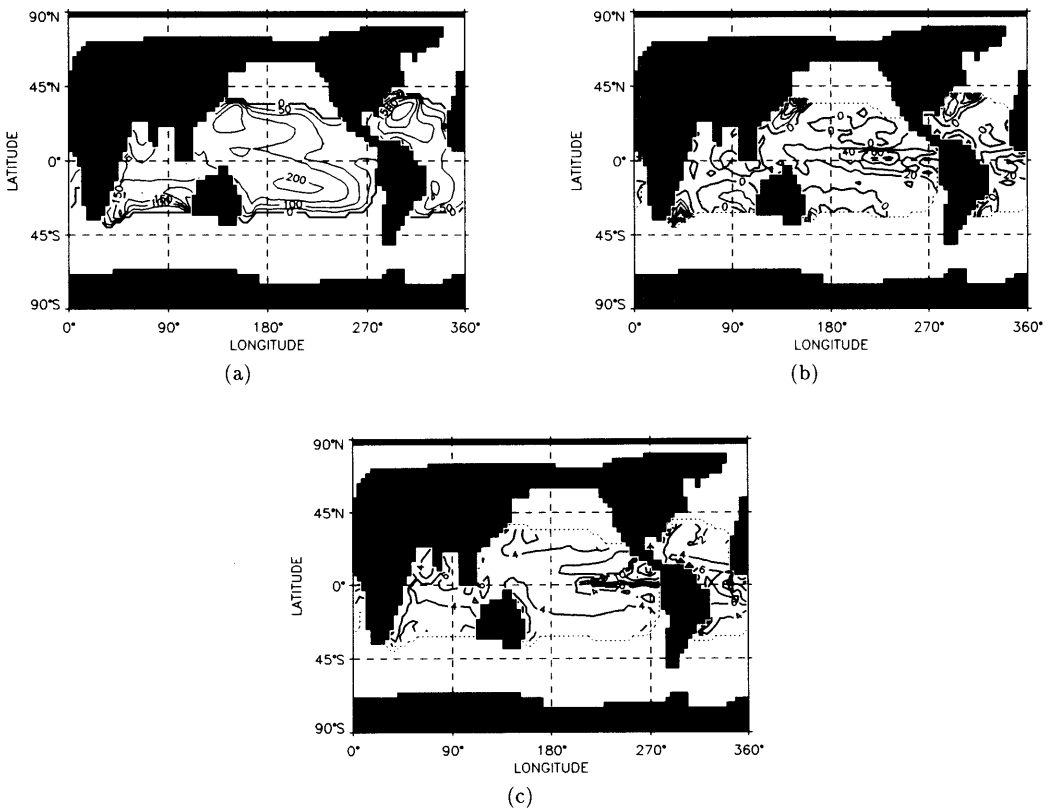

Fig. 6. Fields associated with the heat budget within the $\theta_0 = 20°C$ surface for the solution $\overline{V5}$: (a) h (Contour interval (CI) = 50 m), (b) Q^θ (CI = 20 W m^{-2}), and (c) θ_z at $z = -h$ (CI = 2, scaled by $10^{-2}°C\ m^{-1}$). In (b), shading indicates negative values.

Indian Ocean (with their sum balanced by vertical diffusive cooling), but it only represents about 10% of the balance against surface heating in the Pacific.

For lower θ_0 values all of the ocean basins become connected, so we consider only a global heat budget. With decreasing θ_0, $Q^\theta < 0$ is increasingly prevalent, thus tending to cancel the tropical heating; for $\theta_0 = 10$ and 5°C, for example, the ratios of their total surface forcing to the 20°C value are 65% and 37%, respectively. Furthermore, isotherms and isopycnals become less well aligned in colder water where the salinity makes an increasingly important contribution to determining potential density. Thus isopycnal diffusion plays an increasingly important role in the heat budget; for $\theta_0 = 20$, 10, and 5°C, the ratios of isopycnal diffusion to surface forcing are 4, 19, and 35%, respectively. Finally, the frequency of deep convection through the mean iso-tracer surface increases for colder surfaces. For all these reasons, the onus on vertical mixing in stably stratified fluid to balance the heat budget is far less severe outside the warm water sphere.

We examine the warm water sphere freshwater budgets for isohaline surfaces with $S_0 \geq 35.4$ ppt (Fig. 7). (These budgets are expressed in terms of freshwater fluxes, which are equal to the model salinity fluxes multiplied by $-S_*^{-1}$, where $S_* = 35.0$ is an average salinity value.) The budget volumes are quite different from those for θ, and because the Indonesian passage has relatively fresh S values, the Indian and Pacific Oceans are now analyzed separately. The budget balance (5) shows that surface net evaporation is balanced by significant freshening contributions from both vertical

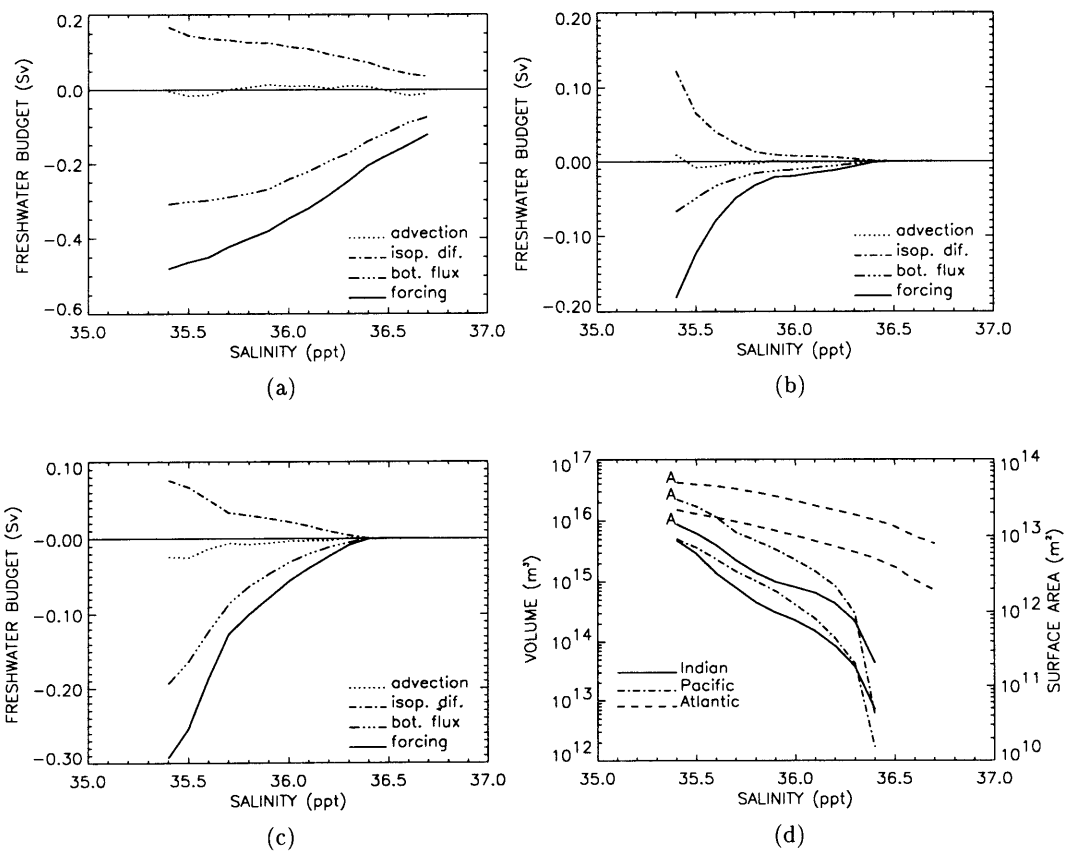

Fig. 7. Freshwater budget as a function of S_0 in (a) Atlantic, (b) Indian, and (c) Pacific basins for the solution $\overline{V5}$. Also shown are (d) the surface area (lines connected to A) and volume contained within the bounding S_0 surface.

and isopycnal fluxes, with the latter the dominant transport mechanism in the Indian Ocean for $S_0 \leqslant 35.7$ (Fig. 7b). This occurs for S, in contrast to θ, because its warm water sphere iso-surfaces are not nearly coincident with isopycnals. Again the discrete advection errors are small, even compared to $\boldsymbol{R}$ here.

Because the Atlantic is much saltier than the other basins (Fig. 7d), we examine the spatial patterns of the budget elements with a larger $S_0 = 35.9$ there than the $S_0 = 35.4$ used in the Indian and Pacific. Their bounding depths are shown in Fig. 8a. They are somewhat deeper than the θ_0 surfaces examined above, particularly in the Indian and Atlantic basins. These volumes are centered on the sub-tropical evaporation zones, with only the north Pacific lacking such a center at this S_0 value. The distribution of surface freshwater flux (i.e., $Q^{H_2O} = -Q^S/S_*$) in Fig. 8b is somewhat noisy, which is an indication of the uncertainty and probable error associated with forcing the model salinity by the restoring boundary condition (see also the discussion in Danabasoglu and McWilliams, 1995). Nevertheless, Q^{H_2O} does show western tropical and western-boundary, mid-latitude precipitation extrema, as well as the broad subtropical regions of strong evaporation. The salinity gradient S_z at the lower boundary (Fig. 8c) is much more uniform than θ_z and tends to be larger in the Southern Hemisphere sub-tropical gyres than elsewhere; its maximum value on this surface is $1.6 \times 10^{-5}\,\mathrm{m}^{-1}$ in the South Atlantic. The isopycnal diffusion horizontal integrand (Fig. 8d) is largest in the sub-tropical boundary

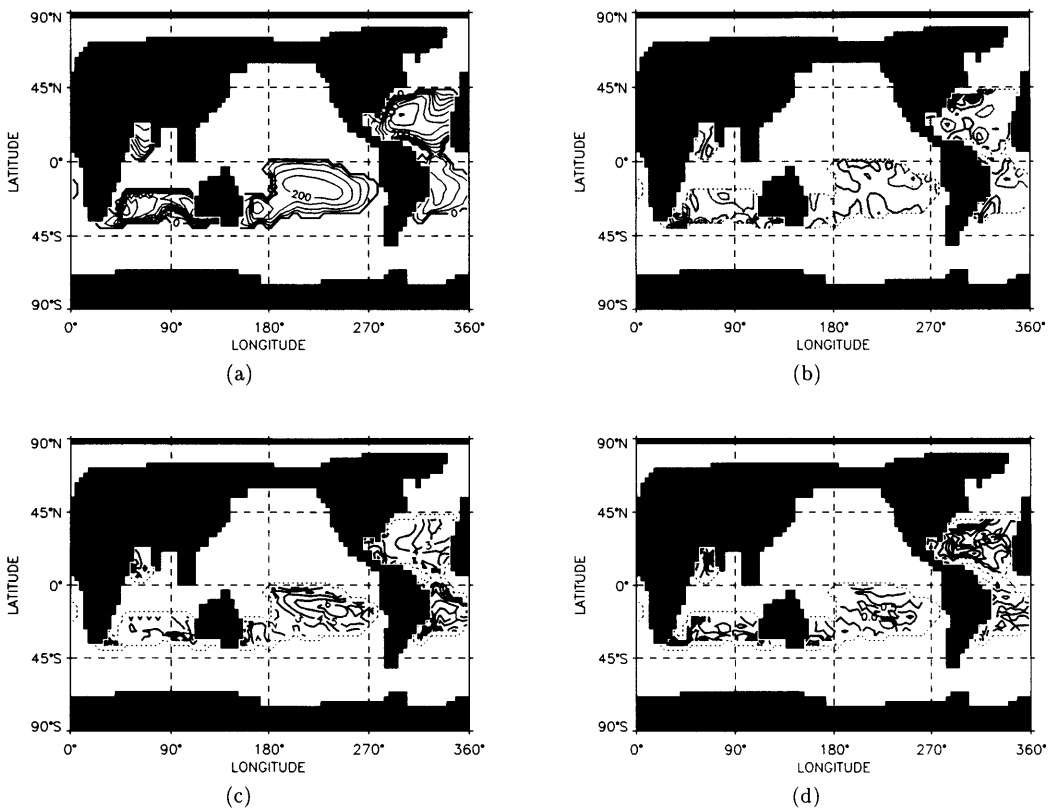

Fig. 8. Fields associated with the freshwater budget within the $S_0 = 35.9$ or 35.4 surfaces (in the Atlantic and Indo-Pacific basins, respectively) for the solution $\overline{V5}$: (a) h (CI = 50 m), (b) Q^{H_2O} (CI = 0.25, scaled by $10^{-7}\,\mathrm{m\,s}^{-1}$), and (c) S_z (CI = 1, scaled by $10^{-6}\,\mathrm{m}^{-1}$) and (d) $-S_*^{-1}\int \mathscr{R}[\kappa_i, S]\,dz$ (CI = 0.5, scaled by $10^{-8}\,\mathrm{m\,s}^{-1}$), both at $z = -h$. In (b) and (d), shading indicates negative values.

currents, where it tends to cancel the precipitation maxima, but it also contributes to the freshening of the subtropical evaporation zones.

We now compare the tracer budgets between the two solutions $\overline{V5}$ and $\overline{V2.5}$. Overall, they are quite similar in the way they satisfy the budget equation (5), and the biggest difference is in the flux magnitudes, as discussed in Section 3 above. The $\overline{V2.5}$ Atlantic heat and freshwater budgets are shown in Fig. 9. They are virtually identical to those of $\overline{V5}$ (Figs. 5a, 7a) except for a change in amplitude. The component heat fluxes are smaller by about a factor of 2/3 with κ_v 1/2 as large, and the freshwater fluxes are smaller by about a factor of 3/4. On average, therefore, the bottom surface gradients have increased by 4/3 and 3/2 for θ_z and S_z, respectively, rather than the doubling that would have kept the vertical diffusive flux constant between cases. Of course, there is an accompanying sharpening of the pycnocline in $\overline{V2.5}$ and a decrease in the depths of budget volumes, although the maximum depth of the $\theta_0 = 20°C$ surface, which occurs in the Sargasso Sea, is nearly unchanged from Fig. 6a. The maximum temperature gradient on the $\theta_0 = 20°C$ surface is $0.23°C\ m^{-1}$ in the Eastern Tropical Pacific, about 5/3 times the maximum in $\overline{V5}$.

The time-mean Atlantic tracer budgets in the solution V5′ are shown in Fig. 10. The time average is taken over only one year, which is sufficient for this almost periodic solution. The budgets are rather similar to those of (Figs. 5a, 7a), consistent with the similarity of their mean tracer

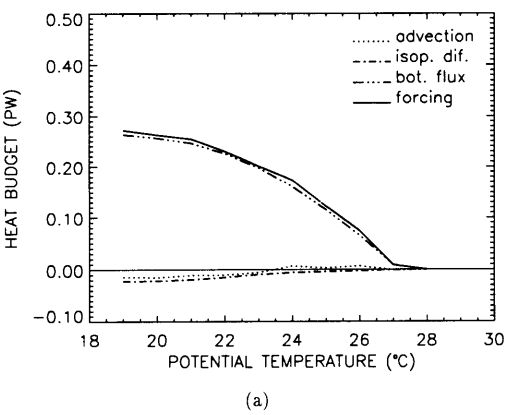

(a)

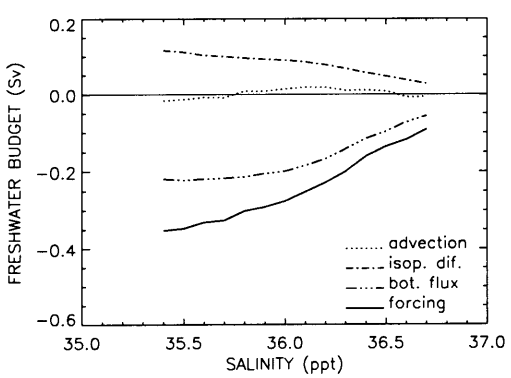

(b)

Fig. 9. Atlantic (a) heat and (b) freshwater budgets as functions of θ_0 and S_0, respectively, for the steady solution with $\kappa_v = 2.5 \times 10^{-5}\ m^2\ s^{-1}$ ($\overline{V2.5}$).

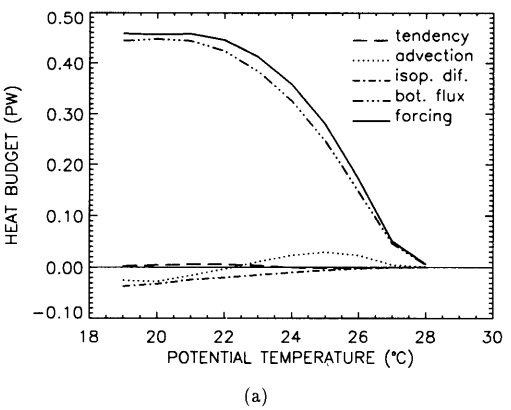

(a)

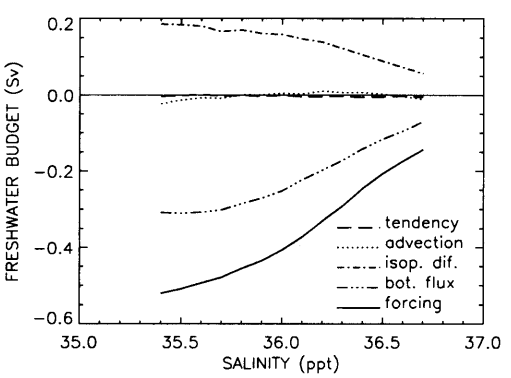

(b)

Fig. 10. One – year time – average Atlantic (a) heat and (b) freshwater budgets as functions of θ_0 and S_0, respectively, for the seasonally varying solution with $\kappa_v = 5 \times 10^{-5}\ m^2\ s^{-1}$ (V5′).

distributions and vertically integrated meridional fluxes (Figs. 2, 3). However, there is a modest increase (by about 10%) in the size of both the surface forcing and vertical bottom flux terms. Also shown in Fig. 10 are the small, but nonzero time-mean contributions from the tracer tendency term; the magnitude, however, is small compared to the discretization error in the budget calculation (i.e., the advection). Rectification as defined in (6) is the source for the tracer tendency term and the augmentation over the corresponding $\overline{V5}$ budget terms. These small but non-trivial rectification terms are shown in Fig. 11: forcing has the largest rectification in the heat budget and isopycnal diffusion the smallest, whereas the opposite is true in the freshwater budget. The rectification occurs with modest amplitude, in part, because the fluctuations in the volume boundaries are not especially large (Fig. 11c). Nevertheless, there is considerable transience in the instantaneous budgets (Fig. 12). The fluctuations in the budget occur primarily with a balance between surface forcing and tracer storage tendency terms.

Some caution should be taken about our demonstration that budget contributions from rectification are modest. They are possibly underestimated in our particular solution because (a) the transient forcing has only seasonal cycle variability, (b) the shallowest model grid cell size is 50 m, whereas much of the true seasonal cycle in

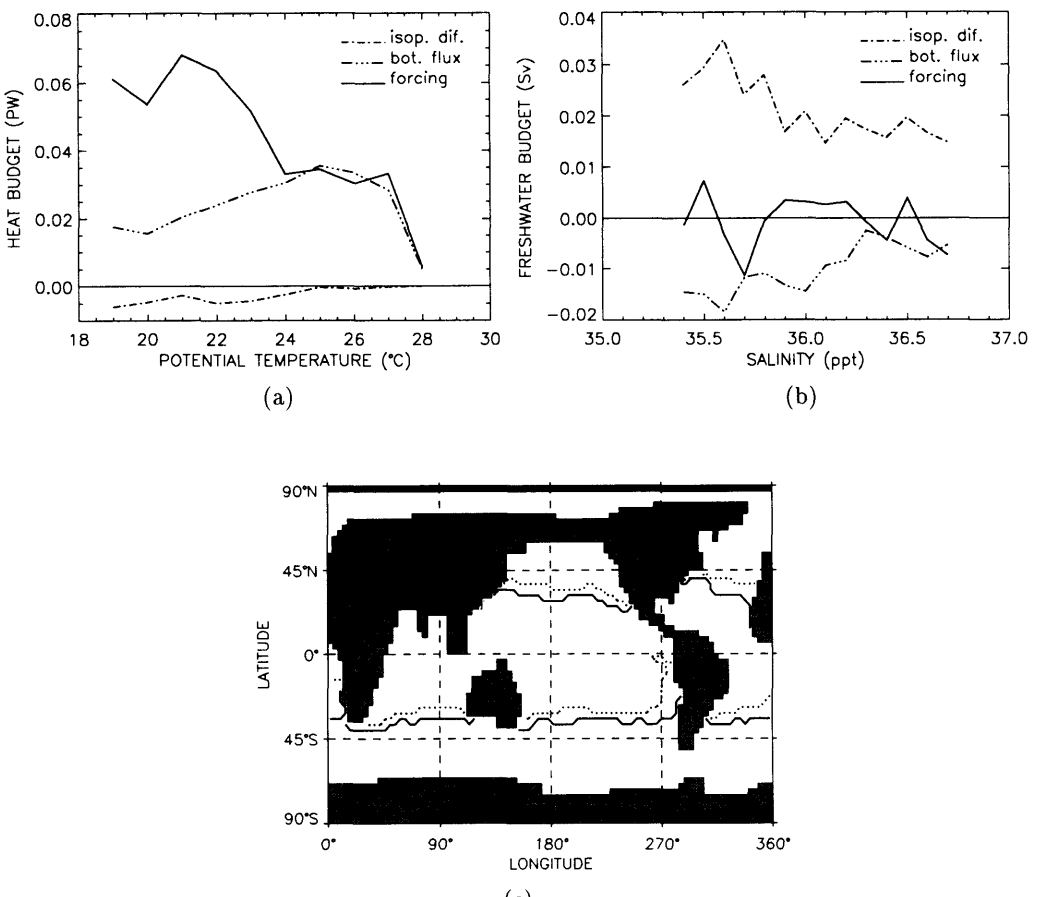

Fig. 11. Rectification contributions RE for the budget terms in Fig. 10 for (a) heat and (b) freshwater. Also shown are (c) the volume boundaries at 25-m depth for the heat budget on day 79 (continuous line) and day 335 (dotted line).

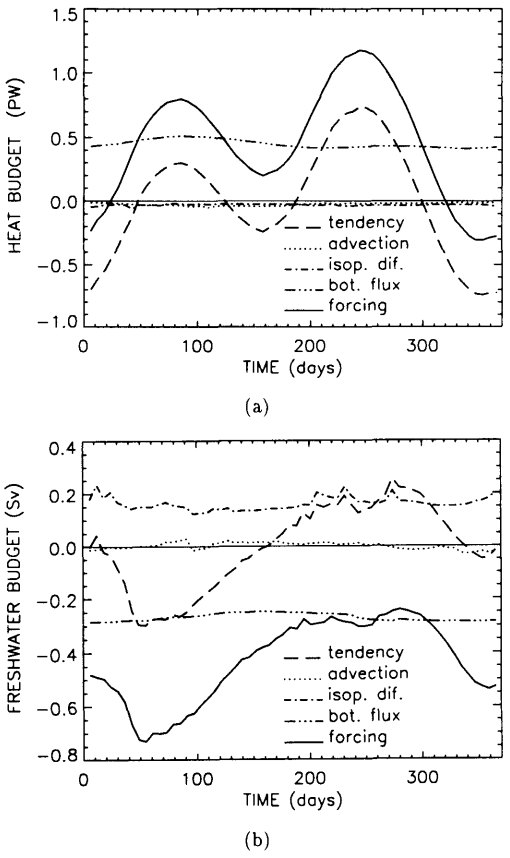

Fig. 12. Seasonal cycle in the (a) heat and (b) freshwater budgets for the $\theta_0 = 20°C$ and $S_0 = 35.9$ surfaces in the Atlantic basin for the solution V5′.

the upper ocean occurs on finer vertical scales, and (c) our solutions exhibit little internal variability due to the constraining surface restoring conditions and large eddy viscosities required by the coarse horizontal resolution.

5. Discussion

In our model solutions the warm water sphere potential temperature and salinity budgets are successfully balanced with small values of diapycnal diffusivity that approach the best present empirical estimates and with approximately the observed surface flux magnitudes. In these budgets, the primary balance is between surface forcing and microscale diapycnal flux across the lower iso-tracer boundary, although mesoscale isopycnal diffusion also plays a significant role for salinity. The time-mean budgets are dominated by contributions from the time-mean interior fluxes and surface forcing, although there are appreciable rectification contributions due to the seasonal cycle.

The present solutions have several qualitative deficiencies compared to the observed general circulation (although they also are significantly improved in this regard because of the isopycnally oriented mesoscale transport parameterization). These include a fresh bias probably associated with inaccurate freshwater surface fluxes, weak gyres and equatorial currents primarily due to coarse horizontal grid resolution, and insufficient seasonal and natural variability because of the constraints of restoring tracer boundary conditions and excessive eddy viscosity (Danabasoglu and McWilliams, 1995). We believe that there is no reason to ascribe any of these deficiencies to the vertical tracer mixing parameterization uniquely. These solutions do not offer any inferential basis for a significant missing process of diapycnal tracer flux, but we would not argue strongly that it cannot exist. This disclaimer is especially applicable to budget volumes outside the warm water sphere whose balances have significant contributions from more processes and therefore pose less of a conundrum a priori and offer a lesser basis for inferences about the role of any particular process. Although numerical models are still relatively simple in their formulation, particularly of the parameterized transport processes, we are prepared to extrapolate our present results to some future calculation with more accurate surface fluxes and more comprehensive and sophisticated treatments of the mesoscale and microscale transport processes, all of which contribute substantially to the tracer dynamics.

Why then have so many empirical budget studies arrived at the different conclusion that κ_v must be $\geqslant 10^{-4}\,m^2\,s^{-1}$ on average? At least for large-scale budgets, a significant difficulty must be in estimating the distribution of vertical tracer gradients on the iso-tracer surfaces. In particular, we have shown that the gradients are quite large in some places (e.g., a θ_z of almost 1°C in 4 m at $\theta_0 = 20°C$ in solution $\overline{V2.5}$), probably much larger than any bulk estimate across the pycnocline. This appears to be the primary difficulty with the κ_v estimates of de Szoeke (1995). Also, of course, the

estimates of surface tracer fluxes are notoriously uncertain, and the large κ_v estimated by Walin (1982) is associated with large Q^θ values. While we are not able to impeach in specific detail all such empirical estimates, we agree with Davis (1994) that the estimation uncertainties in this approach are daunting.

6. Acknowledgements

This research was supported by NSF through its contract with NCAR and by NOAA through grant NA93AANAG0334. We thank Dr. Roland de Szoeke for discussions that stimulated us to investigate this topic.

REFERENCES

Armi, L. 1978. Some evidence for boundary mixing in the deep ocean. *J. Geophys. Res.* **83**, 1971–1979.

Böning, C. W. 1988. Characteristics of particle dispersion in the North Atlantic: an alternative interpretation of SOFAR float results. *Deep-Sea Res.* **35**, 1379–1385.

Bryan, F. 1987. Parameter sensitivity of primitive equation ocean general circulation models. *J. Phys. Ocean.* **17**, 970–985.

Danabasoglu, G., McWilliams, J. C. and Gent, P. R. 1994. The role of mesoscale tracer transports in the global ocean circulation. *Science* **264**, 1123–1126.

Danabasoglu, G. and McWilliams, J. C. 1995. Sensitivity of the global ocean circulation to parameterizations of mesoscale tracer transports. *J. Climate*, in press.

Davis, R. E. 1994. Diapycnal mixing in the ocean: equations for large-scale budgets. *J. Phys. Ocean.* **24**, 777–800.

De Szoeke, R. A. 1995. A model of wind- and buoyancy-driven ocean circulation. *J. Phys. Ocean.* **25**, 918–941.

ECMWF, 1993. The description of the ECMWF/WCRP level III-A global atmospheric data archive. Technical Attachment, ECMWF, 48 p.

Garrett, C. 1991. Marginal mixing theories. *Atmos.-Ocean* **29**, 313–339.

Gent, P. R. and McWilliams, J. C. 1990. Isopycnal mixing in ocean circulation models. *J. Phys. Ocean* **20**, 150–155.

Gent, P. R., Willebrand, J., McDougall, T. J. and McWilliams, J. C. 1995. Parameterizing eddy-induced transports in ocean circulation models. *J. Phys. Ocean.* **25**, 463–474.

Gregg, M. C. 1987. Diapycnal mixing in the thermocline: a review. *J. Geophys. Res.* **92**, 5249–5286.

Hogg, N. G., Biscaye, P., Gardner, W. and Schmitz, W. S. 1982. On the transport and modification of Antarctic Bottom Water in the Vema channel. *J. Marine Res.* **40** (suppl.), 231–263.

Hogg, N. G. 1987. A least-squares fit of the advective-diffusive equations to Levitus Atlas data. *J. Marine Res.* **45**, 347–375.

Ledwell, J. R., Watson, A. J. and Law, C. S. 1993. Evidence for slow mixing across the pycnocline from an open-ocean tracer-release experiment. *Nature* **364**, 701–703.

Ledwell, J. R. and Watson, A. J. 1994. North Atlantic tracer release experiment, newest results. *WOCE Notes* **6**(1), 1–4.

Levitus, S. 1982. *NOAA Professional Paper* 13. US Dept. Commerce Washington, DC.

Li, Y.-H., Peng, T.-H., Broecker, W. S. and Östlund, H. G. 1984. The average vertical mixing coefficient for the ocean thermocline. *Tellus* **36B**, 212–217.

McDougall, T. J. 1987. Neutral surfaces. *J. Phys. Ocean.* **17**, 1950–1964.

McWilliams, J. C., Brown, E. D., Bryden, H. L., Ebbesmeyer, C. C., Elliot, B. A., Heinmiller, R. H., Hua, B. L., Leaman, K. D., Lindstrom, E. J., Luyten, J. R., McDowell, S. E., Owens, W. B., Perkins, H., Price, J. F., Regier, L., Riser, S. C., Rossby, H. T., Sanford, T. B., Shen, C. Y., Taft, B. A. and Van Leer, J. C. 1983. The local dynamics of eddies in the western North Atlantic. *Eddies in Marine Science*, A. R. Robinson, ed. Springer-Verlag, 92–113.

Niiler, P. and Stevenson, J. 1982. The heat budget of tropical ocean warm-water pools. *J. Marine Res.* **40** (suppl.), 465–480.

Olbers, D. J. and Wenzel, M. 1989. Determining diffusivities from hydrographic data by inverse methods with applications to the circumpolar current. *Oceanic circulation Models: data and dynamics*. D.L.T. Anderson and J. Willebrand, eds. Kluwer Academic, 605 p.

Redi, M. H. 1982. Oceanic isopycnal mixing by coordinate rotation. *J. Phys. Ocean* **12**, 1154–1158.

Speer, K. and Tziperman, E. 1992. Rates of water mass formation in the North Atlantic Ocean. *J. Phys. Ocean.* **22**, 93–104.

Toole, J. M., Schmitt, R. W. and Polzin, K. L. 1994. Estimates of diapycnal mixing in the abyssal ocean. *Science* **264**, 1120–1123.

Walin, G. 1982. On the relation between the sea-surface heat flow and thermal circulation in the ocean. *Tellus* **34**, 187–195.

Wüst, G. 1949. Über die Zweiteilung der Hydrosphäre. *Dt. hydrogr. Z.* **2**, 218–225.

Yin, F. L. and Fung, I. 1991. Net diffusivity in ocean general circulation models with nonuniform grids. *J. Geophys. Res.* **96**, 10773–10776.